coatings

MDPI

Communication

Structural and Chemical Peculiarities of Nitrogen-Doped Graphene Grown Using Direct Microwave Plasma-Enhanced Chemical Vapor Deposition

Šarūnas Meškinis, Rimantas Gudaitis, Mindaugas Andrulevičius and Algirdas Lazauskas *

Institute of Materials Science, Kaunas University of Technology, K. Baršausko 59, LT-51423 Kaunas, Lithuania; sarunas.meskinis@ktu.lt (Š.M.); rimantas.gudaitis@ktu.lt (R.G.); mindaugas.andrulevicius@ktu.lt (M.A.)
* Correspondence: algirdas.lazauskas@ktu.edu; Tel.: +370-671-73375

Abstract: Chemical vapor deposition (CVD) is an attractive technique which allows graphene with simultaneous heteroatom doping to be synthesized. In most cases, graphene is grown on a catalyst, followed by the subsequent transfer process. The latter is responsible for the degradation of the carrier mobility and conductivity of graphene due to the presence of the absorbants and transfer-related defects. Here, we report the catalyst-less and transfer-less synthesis of graphene with simultaneous nitrogen doping in a single step at a reduced temperature (700 °C) via the use of direct microwave plasma-enhanced CVD. By varying nitrogen flow rate, we explored the resultant structural and chemical properties of nitrogen-doped graphene. Atomic force microscopy revealed a more distorted growth process of graphene structure with the introduction of nitrogen gas—the root mean square roughness increased from 0.49 ± 0.2 nm to 2.32 ± 0.2 nm. Raman spectroscopy indicated that nitrogen-doped, multilayer graphene structures were produced using this method. X-ray photoelectron spectroscopy showed the incorporation of pure pyridinic N dopants into the graphene structure with a nitrogen concentration up to 2.08 at.%.

Keywords: microwave; plasma-enhanced; CVD; nitrogen-doped; graphene; catalyst-less; transfer-less; synthesis

Citation: Meškinis, Š.; Gudaitis, R.; Andrulevičius, M.; Lazauskas, A. Structural and Chemical Peculiarities of Nitrogen-Doped Graphene Grown Using Direct Microwave Plasma-Enhanced Chemical Vapor Deposition. *Coatings* **2022**, *12*, 572. https://doi.org/10.3390/coatings12050572

Academic Editor: Luca Valentini

Received: 29 March 2022
Accepted: 20 April 2022
Published: 22 April 2022

1. Introduction

Graphene belongs to a class of two-dimensional (2D) materials, which are widely known for their unique structures and outstanding physical, chemical, and mechanical properties [1–7]. It was demonstrated in many studies and reviews that the properties of 2D materials can be drastically altered, enhanced, or tuned via molecular and atomic doping [8–11]. For instance, the carrier concentration and type of carrier can be easily changed through the substitution of dopant atoms on the sulfur site in titanium trisulfide without having any impact on the band extrema [12]. After doping carbon nanotubes with N or B atoms, they become n-type or p-type atoms, respectively [13]. Doped graphene offers unique properties such as ferromagnetism [14], superconductivity [15], etc. Specifically, graphene heteroatom doping methods can be categorized [16] into post-treatment approaches, e.g., wet chemical methods [17], thermal annealing, arc-discharge [18], plasma treatment [19], hydrothermal treatment [20], and gamma irradiation [21], and in situ approaches, e.g., chemical vapor deposition (CVD) [22], bottom-up synthesis [23], and ball milling [24]. Methods which fall into the latter category are more favorable, as graphene synthesis can be achieved with simultaneous heteroatom doping [16]. Depending on the choice of heteroatoms for doping, e.g., B [25], N [26], P [27], S [28], F [29], Cl [30], Br [31], I [32], etc., new or improved properties of graphene materials may arise and could be useful for a number of applications, including supercapacitors [33], fuel cells [34], lithium ion batteries [35], solar cells [36], and sensors [37].

The CVD technique can be considered as the most effective approach used for graphene doping that does not affect its crystalline nature [38]. Generally, graphene is grown via CVD on a catalyst substrate, e.g., Ni or Cu [39,40], and afterwards, a complicated transfer process is required for the wet chemical removal of the metallic catalyst and the transfer of the graphene onto the required surface based on its intended functionality and application [41]. Importantly, the transfer process is known to be responsible for the generation of defects and the degradation of the carrier mobility and conductivity of graphene, since chemical alterations (i.e., during the wet chemical removal of catalyst) and mechanical damage (i.e., during the transfer process) are almost unavoidable during this process [42]. Additionally, the graphene transfer process is known to introduce unwanted metallic impurities which alter the electrochemical properties of graphene [43]. The demand for monocrystalline Si(1 0 0) continues to rise, as it is a major substrate used in semiconductor device fabrication and optoelectronics. The catalyst-less and transfer-less synthesis of graphene on monocrystalline Si(1 0 0) is meaningful in this context.

Herein, we focused our efforts on demonstrating that the catalyst-less and transfer-less synthesis of graphene can be achieved with simultaneous nitrogen doping in a single step via the use of a direct microwave plasma-enhanced CVD. Importantly, nitrogen-doped graphene synthesis was achieved at a considerably low temperature of 700 °C. By varying nitrogen flow rate, we explored the resultant structural and chemical properties of nitrogen-doped graphene through atomic force microscopy (AFM), Raman spectroscopy, and X-ray photoelectron spectroscopy (XPS).

2. Materials and Methods

2.1. Microwave Plasma-Enhanced CVD of Nitrogen-Doped Graphene

The direct transfer-less synthesis of nitrogen-doped graphene was performed by employing the microwave plasma-enhanced CVD system Cyrannus (Innovative Plasma Systems (Iplas) GmbH, Troisdorf, Germany). Monocrystalline Si(1 0 0) (UniversityWafer Inc., South Boston, MA, USA) was used as a substrate. Plasma cleaning (power 1.7 kW, operating pressure 22 mbar, temperature 700 °C, hydrogen flow rate 200 sccm, and process duration 10 min) of the substrate was performed until the heater reached the target temperature. A methane, hydrogen, and nitrogen gas mixture was used for the direct synthesis of nitrogen-doped graphene. Afterwards, methane and nitrogen gas were introduced into the chamber. The growth process was performed in a single step. A steel enclosure on the substrate was used for the elimination of the unwanted direct plasma effects. The technological parameters of the plasma (i.e., power 0.7 kW, operating pressure 20 mbar, temperature 700 °C, and process duration 60 min) and the flow rate of hydrogen (75 sccm) and methane (35 sccm) gases were kept constant, while the flow rate of nitrogen gas was varied in the range of 0–110 sccm. Samples were denoted depending on the flow rate of nitrogen used in the process: N0 (N_2, 0 sccm), N35 (N_2, 35 sccm), N75 (N_2, 75 sccm), or N110 (N_2, 110 sccm).

2.2. Characterization

A NanoWizardIII atomic force microscope (JPK Instruments, Bruker Nano GmbH, Berlin, Germany) was used to conduct experiments at room temperature, with data analyzed using a SurfaceXplorer and JPKSPM Data Processing software (Version spm-4.3.13, JPK Instruments, Bruker Nano GmbH). An ACTA probe (Applied NanoStructures, Inc., Mountain View, CA, USA, specification: cantilever shape—pyramidal; radius of curvature < 10.0 nm and cone angle—20°; calibrated spring constant—54.2 N/m; reflex side coating—Al with thickness of 50 nm ± 5 nm) was used to acquire AFM topographical images in contact mode.

Raman spectroscopy was performed using an inVia Raman spectrometer (Renishaw, Wotton-under-Edge, UK) equipped with a semiconductor green laser (wavelength of 532 nm), 2400 lines/mm grating, confocal microscope (50× objective), and CCD camera. The 5% laser output power was used for spectra recording (10 × 10 s accumulation time)

in order to avoid sample damage. Band deconvolution into separate components was performed with OriginPro 8.0 software (OriginLab, Northampton, MA, USA).

Chemical state changes were investigated by employing a Thermo Scientific ESCALAB 250Xi spectrometer with monochromatized Al Kα radiation (hν = 1486.6 eV): X-ray spot of 0.9 mm in diameter; base pressure better than 3×10^{-9} Torr; 40 eV pass energy in transmission mode; energy scale calibration according to Au $4f_{7/2}$, Ag $3d_{5/2}$ and Cu $2p_{3/2}$. The peak fitting procedure was performed using the original ESCALAB 250Xi Avantage software.

3. Results and Discussion

The AFM analysis of pristine graphene (Figure 1a) was conducted over a 1.1×1.1 μm^2 area for quantitative morphological evaluation. The pristine graphene surface had a random distribution of surface features (mean height, Z_{mean} of 0.76 ± 0.2 nm) with varying angle orientation to each other, without a preferred direction. The root mean square roughness (R_q) was determined to be 0.16 ± 0.2 nm. The skewness (R_{sk}) was determined to be 0.19 ± 0.2, indicating that the surface peaks dominate over the valleys. The pristine graphene surface exhibited a leptokurtoic distribution of surface features with a kurtosis (R_{ku}) value of 3.32 ± 0.2.

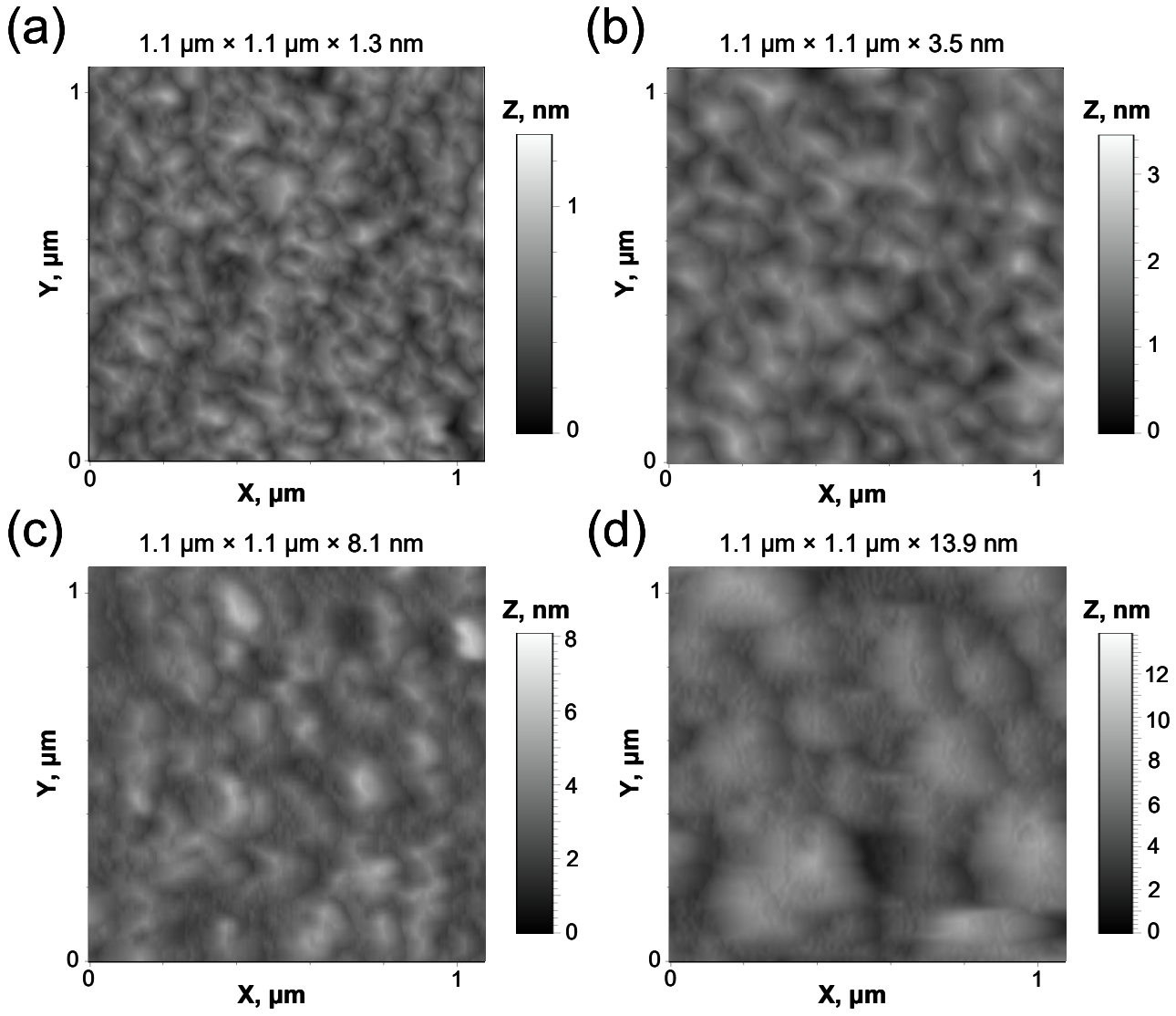

Figure 1. AFM surface topography of pristine graphene (**a**), N35 (**b**), N75 (**c**), and N110 (**d**).

Some significant changes in surface topography (Figure 1b–d) as well as morphology (Table 1) can be observed for nitrogen-doped graphene: with the increase in nitrogen flow rate, the grain-like surface feature size increases in dimensions, with deeper valleys formed in between the boundaries (Figure S1). In general, the height of the surface structures and the roughness increase with the nitrogen flow rate. This change can be explained by the collision between nitrogen and carbon atoms as well as inner atom substitutional placement in the sp^2 hybridized lattice that results in the formation of various nitrogen-induced defect complexes [44], which evidently leads to a more distorted growth process of the graphene structure. Furthermore, graphene synthesis is performed in hydrogen plasma, which is also known to be responsible for defect formation [45,46]. Figure S2 shows the AFM step profiles for the corresponding samples. The thickness of the synthesized graphene films was found to be in the range of 9–13 ± 1 nm with no clear dependence on the nitrogen gas flow rate.

Table 1. Surface morphological parameters.

Sample No.	Morphological Parameter			
	Z_{mean}, nm	R_q, nm	R_{sk}	R_{ku}
N0	0.76 ± 0.2	0.16 ± 0.2	0.19 ± 0.2	3.32 ± 0.2
N35	1.65 ± 0.2	0.49 ± 0.2	0.35 ± 0.2	3.09 ± 0.2
N75	3.12 ± 0.2	1.33 ± 0.2	0.93 ± 0.2	4.12 ± 0.2
N110	7.30 ± 0.2	2.32 ± 0.2	0.18 ± 0.2	3.14 ± 0.2

Figure 2 shows Raman spectra of pristine graphene grown directly on monocrystalline Si(1 0 0) substrate, as well as nitrogen-doped graphene samples. Raman spectra are presented in two actual wavenumber ranges of 1100–1800 cm^{-1} and 2450–3150 cm^{-1}, respectively. Four deconvoluted bands were determined using Gaussian components consisting of D and G bands at 1347 cm^{-1} and 1599 cm^{-1} and 2D and G + D bands at 2687 cm^{-1} and 2937 cm^{-1} for pristine graphene. The high I_D/I_G ratio of 1.26 indicates highly defective graphene. The low I_{2D}/I_G (0.15) and the broad 2D band in the Raman spectrum indicates the multilayer structure of graphene. The nitrogen doping of graphene is confirmed by the increased I_D/I_G ratio of samples N35 and N75 (Figure 2b,c), as well as the blue shift of the G band position at 1596 and 1595 cm^{-1} for N75 and N110 (Figure 2c,d), respectively. Additionally, a red shift of the 2D position is observed for N110. Previously, Raman studies of nitrogen-doped graphene were conducted in depth to explain the red and blue shift behavior of 2D and G peak positions, corresponding to n-type doping and compressive/tensile strain in graphene [38,44,47]. S. Zheng et al. investigated the metal-catalyst-free growth of graphene on insulating substrates via ammonia-assisted microwave plasma-enhanced CVD [48]. They also observed the blue shift of the G peak position for nitrogen-doped graphene samples.

XPS was employed for the investigation of chemical state changes in the graphene structure resulting from the nitrogen doping. Figure S3 shows high-resolution XPS spectra in C 1s region for pristine graphene, N35 and N110, respectively. The deconvolution of spectra for these samples showed similar results: the strongest component at 284.2 eV, a less intense component at 284.8 eV, and a low-intensity component at 285.7 eV. A highly asymmetric component at 284.2 eV was assigned to C–C (sp^2) bonds [22,49]. The second component at 284.6 eV was assigned to C–C (sp^3) bonds [22,50]. The low-intensity component at 285.7 eV was assigned to C–O–C bonds [51,52]. It was found that the sp^2/sp^3 ratio decreased with nitrogen gas flow rate (Figure S3). Figure 3a does not indicate nitrogen-related peaks in the high-resolution N 1s spectrum, confirming the pristine nature of graphene. Figure 3b,c show the high-resolution XPS N 1s spectra with deconvoluted components of N35 and N110. The deconvoluted components in the high-resolution XPS N 1s spectra were attributed to pyridinic N (398.9 eV and 398.6 eV) [53,54], sp^2 C–N bonds (398.0 eV and 397.8 eV) [55,56], and N–Si bonds (397.2 eV and 397.0 eV) [57,58]. The latter comes from the contribution of the substrate as nitrogen-doped graphene was grown di-

rectly on monocrystalline Si(1 0 0). It is also important to note that the sp^2 C–N bonding configuration is similar to pyridine. On the basis of these results, it was determined that the direct microwave plasma-enhanced CVD process produced graphene doped with pure pyridinic N. It was previously reported that the pyridinic N dopant efficiently changes the structure of the graphene valence band, including increasing the density of π states near the Fermi level, as well as reducing work function [59]. Lower work function can dramatically enhance the emitting current in graphene-based electronic devices [60]. It was also demonstrated in [61] that pyridinic nitrogen configuration in graphene contributed to the high catalytic performance. D. Wei et al. investigated the low-temperature critical growth of nitrogen-doped graphene on dielectrics via plasma-enhanced CVD [62]. They also found that nitrogen atoms in graphene are mainly bonded in the pyridinic N form (i.e., a nitrogen atom with two carbon atom neighbors assembling a hexagonal ring). The results of the atomic concentration calculation (Table 2) showed an increase in nitrogen from 1.04 at.% to 2.08 at.% for N35 and N110, respectively, indicating an increased level of pyridinic N doping with an increase in nitrogen gas flow rate. A very similar nitrogen concentration (i.e., 2.0 at.%) was reported for nitrogen-doped graphene synthesized using the N_2:CH_4 ratio of 2:1 via the direct microwave plasma-enhanced CVD process [44]. A nitrogen concentration of 2.0 at.% was also reported for nitrogen-doped graphene synthesized using a camphor:melamine ratio of 1:3 via the atmospheric pressure CVD process [38].

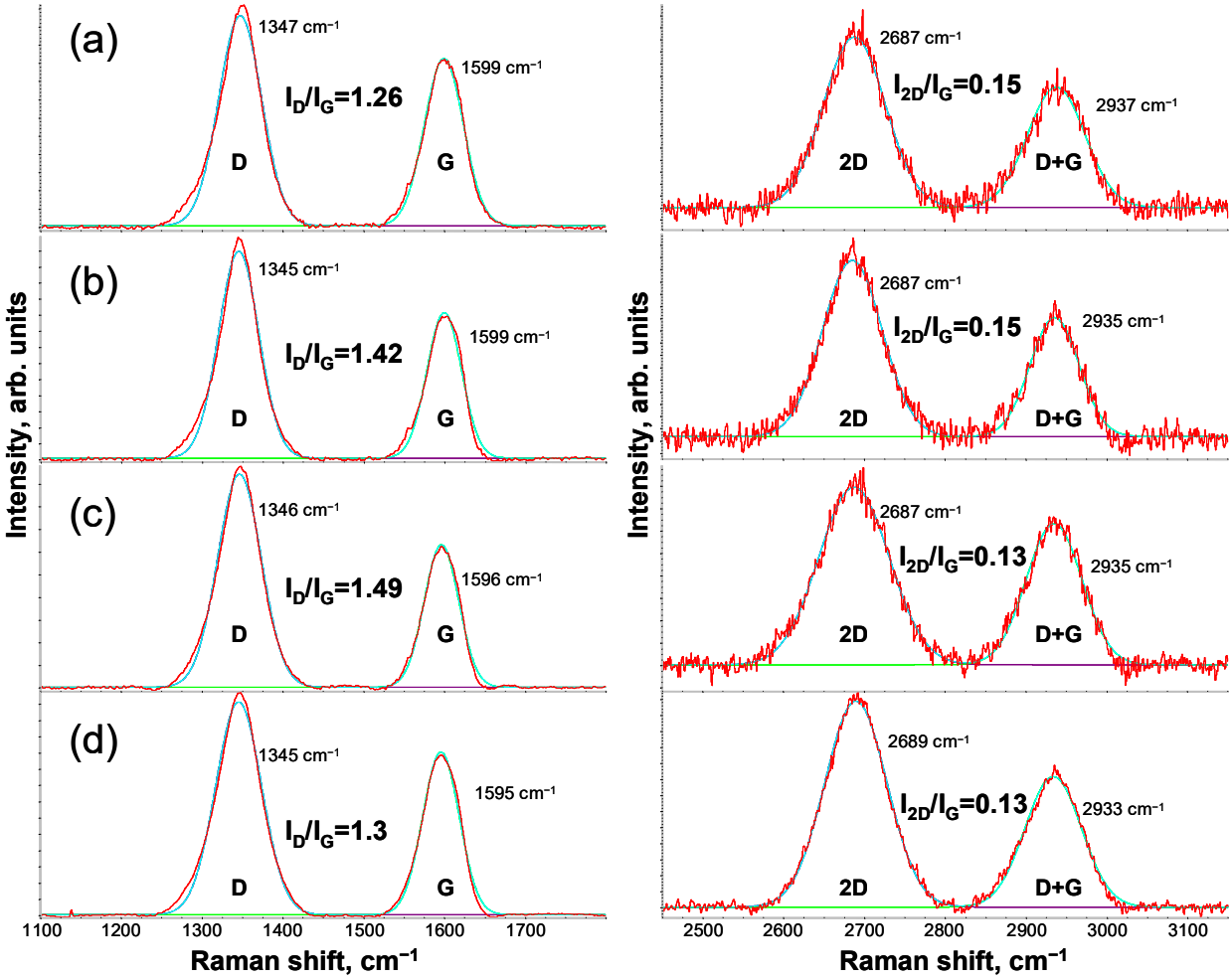

Figure 2. Raman spectra of pristine graphene (**a**), N35 (**b**), N75 (**c**), and N110 (**d**) recorded at 532 nm excitation wavelength and presented in two actual wavenumber ranges.

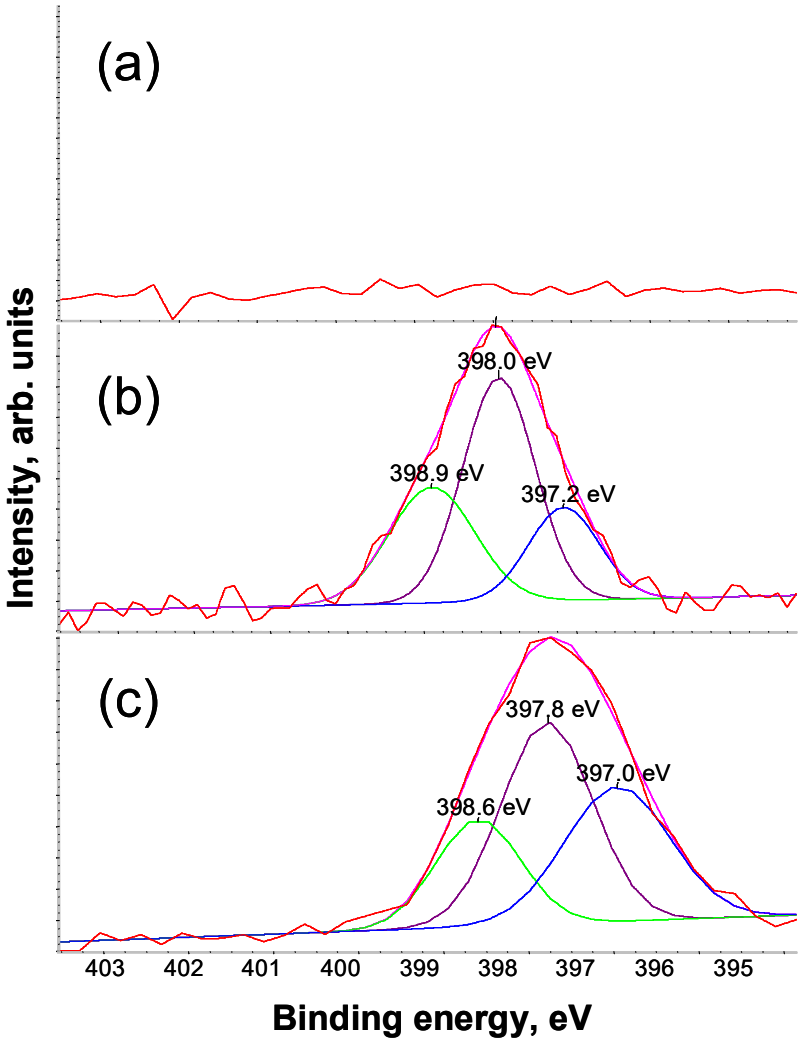

Figure 3. Deconvoluted high-resolution XPS spectra in N 1s region of pristine graphene (**a**), N35 (**b**), and N110 (**c**).

Table 2. Atomic concentration calculation results.

Peak	Atomic Concentration (%)		
	N0	**N35**	**N100**
O 1s	18.48	21.25	21.63
N 1s	0	1.04	2.08
C 1s	47.69	36.37	36.29
Si 2p	33.83	41.35	40

4. Conclusions

We demonstrated the catalyst-less and transfer-less synthesis of nitrogen-doped graphene in a single step at a reduced temperature of 700 °C by using direct microwave plasma-enhanced CVD. The nitrogen flow rate was varied to explore the structural and chemical peculiarities of nitrogen-doped graphene. AFM analysis showed that the height of the graphene surface structures and the roughness increase with the nitrogen flow rate due to nitrogen-induced defect complexes, which evidently lead to a more distorted growth process of the planar graphene. These structural changes were also quantified via Raman spectroscopy. Furthermore, it was determined that nitrogen-doped multilayer graphene structures were produced using this method. XPS analysis showed that pure pyridinic

N was incorporated into the graphene structure during the simultaneous doping process. The level of pyridinic N doping increased with the nitrogen gas flow rate. Nitrogen-doped graphene could have potential applications in optoelectronics.

Supplementary Materials: The following are available online at https://www.mdpi.com/article/10.3390/coatings12050572/s1. Figure S1: Characteristic height profiles for the corresponding lines drawn in AFM images of pristine graphene (a), N35 (b), N75 (c), and N110 (d), Figure S2: Characteristic step profiles for the corresponding lines drawn in AFM images of pristine graphene (a), N35 (b), N75 (c), and N110 (d), Figure S3: Deconvoluted high-resolution XPS spectra in C 1s region of N0, N35, and N110.

Author Contributions: Conceptualization, R.G., Š.M. and A.L.; investigation, R.G., A.L., Š.M. and M.A.; writing—original draft preparation, Š.M. and A.L.; writing—review and editing, A.L. and Š.M.; visualization, A.L.; project administration, Š.M.; funding acquisition, Š.M. All authors have read and agreed to the published version of the manuscript.

Funding: This research was (and is) funded by the European Social Fund under the No. 09.3.3-LMT-K-712-01 "Improvement of researchers' qualification by implementing world-class R&D projects" measure. Grant No. 09.3.3-LMT-K-712-01-0183.

Institutional Review Board Statement: Not applicable.

Informed Consent Statement: Not applicable.

Data Availability Statement: Not applicable.

Acknowledgments: A special thanks go to A. Vasiliauskas, A. Guobienė, K. Šlapikas, V. Stankus, D. Peckus, E. Rajackaitė, T. Tamulevičius, A. Jurkevičiūtė, Š. Jankauskas, and F. Kalyk for technical assistance.

Conflicts of Interest: The authors declare no conflict of interest.

References

1. Mas-Balleste, R.; Gomez-Navarro, C.; Gomez-Herrero, J.; Zamora, F. 2D materials: To graphene and beyond. *Nanoscale* **2011**, *3*, 20–30. [CrossRef] [PubMed]
2. Maniadi, A.; Vamvakaki, M.; Suchea, M.; Tudose, I.V.; Popescu, M.; Romanitan, C.; Pachiu, C.; Ionescu, O.N.; Viskadourakis, Z.; Kenanakis, G. Effect of graphene nanoplatelets on the structure, the morphology, and the dielectric behavior of low-density polyethylene nanocomposites. *Materials* **2020**, *13*, 4776. [CrossRef] [PubMed]
3. Wang, Q.H.; Kalantar-Zadeh, K.; Kis, A.; Coleman, J.N.; Strano, M.S. Electronics and optoelectronics of two-dimensional transition metal dichalcogenides. *Nat. Nanotechnol.* **2012**, *7*, 699–712. [CrossRef] [PubMed]
4. Poot, M.; van der Zant, H.S. Nanomechanical properties of few-layer graphene membranes. *Appl. Phys. Lett.* **2008**, *92*, 063111. [CrossRef]
5. Butler, S.Z.; Hollen, S.M.; Cao, L.; Cui, Y.; Gupta, J.A.; Gutiérrez, H.R.; Heinz, T.F.; Hong, S.S.; Huang, J.; Ismach, A.F. Progress, challenges, and opportunities in two-dimensional materials beyond graphene. *ACS Nano* **2013**, *7*, 2898–2926. [CrossRef]
6. Sun, P.; Wang, K.; Zhu, H. Recent developments in graphene-based membranes: Structure, mass-transport mechanism and potential applications. *Adv. Mater.* **2016**, *28*, 2287–2310. [CrossRef]
7. Akinwande, D.; Brennan, C.J.; Bunch, J.S.; Egberts, P.; Felts, J.R.; Gao, H.; Huang, R.; Kim, J.-S.; Li, T.; Li, Y. A review on mechanics and mechanical properties of 2D materials—Graphene and beyond. *Extrem. Mech. Lett.* **2017**, *13*, 42–77. [CrossRef]
8. Maiti, U.N.; Lee, W.J.; Lee, J.M.; Oh, Y.; Kim, J.Y.; Kim, J.E.; Shim, J.; Han, T.H.; Kim, S.O. 25th anniversary article: Chemically modified/doped carbon nanotubes & graphene for optimized nanostructures & nanodevices. *Adv. Mater.* **2014**, *26*, 40–67.
9. Lv, R.; Terrones, M. Towards new graphene materials: Doped graphene sheets and nanoribbons. *Mater. Lett.* **2012**, *78*, 209–218. [CrossRef]
10. Georgakilas, V.; Otyepka, M.; Bourlinos, A.B.; Chandra, V.; Kim, N.; Kemp, K.C.; Hobza, P.; Zboril, R.; Kim, K.S. Functionalization of graphene: Covalent and non-covalent approaches, derivatives and applications. *Chem. Rev.* **2012**, *112*, 6156–6214. [CrossRef]
11. Dong, X.; Long, Q.; Wei, A.; Zhang, W.; Li, L.-J.; Chen, P.; Huang, W. The electrical properties of graphene modified by bromophenyl groups derived from a diazonium compound. *Carbon* **2012**, *50*, 1517–1522. [CrossRef]
12. Tripathi, N.; Pavelyev, V.; Sharma, P.; Kumar, S.; Rymzhina, A.; Mishra, P. Review of titanium trisulfide (TiS3): A novel material for next generation electronic and optical devices. *Mater. Sci. Semicond. Process.* **2021**, *127*, 105699. [CrossRef]
13. Wei, D.; Liu, Y.; Wang, Y.; Zhang, H.; Huang, L.; Yu, G. Synthesis of N-doped graphene by chemical vapor deposition and its electrical properties. *Nano Lett.* **2009**, *9*, 1752–1758. [CrossRef]
14. Peres, N.; Guinea, F.; Neto, A.C. Coulomb interactions and ferromagnetism in pure and doped graphene. *Phys. Rev. B* **2005**, *72*, 174406. [CrossRef]

15. Uchoa, B.; Neto, A.C. Superconducting states of pure and doped graphene. *Phys. Rev. Lett.* **2007**, *98*, 146801. [CrossRef] [PubMed]
16. Wang, X.; Sun, G.; Routh, P.; Kim, D.-H.; Huang, W.; Chen, P. Heteroatom-doped graphene materials: Syntheses, properties and applications. *Chem. Soc. Rev.* **2014**, *43*, 7067–7098. [CrossRef] [PubMed]
17. Wu, P.; Cai, Z.; Gao, Y.; Zhang, H.; Cai, C. Enhancing the electrochemical reduction of hydrogen peroxide based on nitrogen-doped graphene for measurement of its releasing process from living cells. *Chem. Commun.* **2011**, *47*, 11327–11329. [CrossRef]
18. Li, N.; Wang, Z.; Zhao, K.; Shi, Z.; Gu, Z.; Xu, S. Large scale synthesis of N-doped multi-layered graphene sheets by simple arc-discharge method. *Carbon* **2010**, *48*, 255–259. [CrossRef]
19. Jeong, H.M.; Lee, J.W.; Shin, W.H.; Choi, Y.J.; Shin, H.J.; Kang, J.K.; Choi, J.W. Nitrogen-doped graphene for high-performance ultracapacitors and the importance of nitrogen-doped sites at basal planes. *Nano Lett.* **2011**, *11*, 2472–2477. [CrossRef]
20. Ion-Ebrașu, D.; Andrei, R.D.; Enache, S.; Căprărescu, S.; Negrilă, C.C.; Jianu, C.; Enache, A.; Boerașu, I.; Carcadea, E.; Varlam, M. Nitrogen functionalization of cvd grown three-dimensional graphene foam for hydrogen evolution reactions in alkaline media. *Materials* **2021**, *14*, 4952. [CrossRef]
21. Kamedulski, P.; Truszkowski, S.; Lukaszewicz, J.P. Highly effective methods of obtaining N-doped graphene by gamma irradiation. *Materials* **2020**, *13*, 4975. [CrossRef] [PubMed]
22. Komissarov, I.V.; Kovalchuk, N.G.; Labunov, V.A.; Girel, K.V.; Korolik, O.V.; Tivanov, M.S.; Lazauskas, A.; Andrulevičius, M.; Tamulevičius, T.; Grigaliūnas, V. Nitrogen-doped twisted graphene grown on copper by atmospheric pressure CVD from a decane precursor. *Beilstein J. Nanotechnol.* **2017**, *8*, 145–158. [CrossRef] [PubMed]
23. Lü, X.; Wu, J.; Lin, T.; Wan, D.; Huang, F.; Xie, X.; Jiang, M. Low-temperature rapid synthesis of high-quality pristine or boron-doped graphene via Wurtz-type reductive coupling reaction. *J. Mater. Chem.* **2011**, *21*, 10685–10689. [CrossRef]
24. Jeon, I.-Y.; Choi, H.-J.; Ju, M.J.; Choi, I.T.; Lim, K.; Ko, J.; Kim, H.K.; Kim, J.C.; Lee, J.-J.; Shin, D. Direct nitrogen fixation at the edges of graphene nanoplatelets as efficient electrocatalysts for energy conversion. *Sci. Rep.* **2013**, *3*, 2260. [CrossRef]
25. Rani, P.; Jindal, V. Designing band gap of graphene by B and N dopant atoms. *RSC Adv.* **2013**, *3*, 802–812. [CrossRef]
26. Lherbier, A.; Botello-Méndez, A.R.; Charlier, J.-C. Electronic and transport properties of unbalanced sublattice N-doping in graphene. *Nano Lett.* **2013**, *13*, 1446–1450. [CrossRef]
27. Liu, Z.W.; Peng, F.; Wang, H.J.; Yu, H.; Zheng, W.X.; Yang, J. Phosphorus-doped graphite layers with high electrocatalytic activity for the O_2 reduction in an alkaline medium. *Angew. Chem. Int. Ed.* **2011**, *50*, 3257–3261. [CrossRef]
28. Denis, P.A. Band gap opening of monolayer and bilayer graphene doped with aluminium, silicon, phosphorus, and sulfur. *Chem. Phys. Lett.* **2010**, *492*, 251–257. [CrossRef]
29. Ribas, M.A.; Singh, A.K.; Sorokin, P.B.; Yakobson, B.I. Patterning nanoroads and quantum dots on fluorinated graphene. *Nano Res.* **2011**, *4*, 143–152. [CrossRef]
30. Yang, M.; Zhou, L.; Wang, J.; Liu, Z.; Liu, Z. Evolutionary chlorination of graphene: From charge-transfer complex to covalent bonding and nonbonding. *J. Phys. Chem. C* **2012**, *116*, 844–850. [CrossRef]
31. Venkatesan, N.; Archana, K.S.; Suresh, S.; Aswathy, R.; Ulaganthan, M.; Periasamy, P.; Ragupathy, P. Boron-Doped Graphene as Efficient Electrocatalyst for Zinc-Bromine Redox Flow Batteries. *ChemElectroChem* **2019**, *6*, 1107–1114. [CrossRef]
32. Kalita, G.; Wakita, K.; Takahashi, M.; Umeno, M. Iodine doping in solid precursor-based CVD growth graphene film. *J. Mater. Chem.* **2011**, *21*, 15209–15213. [CrossRef]
33. Yu, X.; Li, N.; Zhang, S.; Liu, C.; Chen, L.; Xi, M.; Song, Y.; Ali, S.; Iqbal, O.; Han, M. Enhancing the energy storage capacity of graphene supercapacitors via solar heating. *J. Mater. Chem. A* **2022**, *10*, 3382–3392. [CrossRef]
34. Chen, J.; Bailey, J.J.; Britnell, L.; Perez-Page, M.; Sahoo, M.; Zhang, Z.; Strudwick, A.; Hack, J.; Guo, Z.; Ji, Z. The performance and durability of high-temperature proton exchange membrane fuel cells enhanced by single-layer graphene. *Nano Energy* **2022**, *93*, 106829. [CrossRef]
35. Mu, Y.; Han, M.; Li, J.; Liang, J.; Yu, J. Growing vertical graphene sheets on natural graphite for fast charging lithium-ion batteries. *Carbon* **2021**, *173*, 477–484. [CrossRef]
36. Safie, N.E.; Azam, M.A.; Aziz, M.F.; Ismail, M. Recent progress of graphene-based materials for efficient charge transfer and device performance stability in perovskite solar cells. *Int. J. Energy Res.* **2021**, *45*, 1347–1374. [CrossRef]
37. Xie, T.; Wang, Q.; Wallace, R.M.; Gong, C. Understanding and optimization of graphene gas sensors. *Appl. Phys. Lett.* **2021**, *119*, 013104. [CrossRef]
38. Shinde, S.M.; Kano, E.; Kalita, G.; Takeguchi, M.; Hashimoto, A.; Tanemura, M. Grain structures of nitrogen-doped graphene synthesized by solid source-based chemical vapor deposition. *Carbon* **2016**, *96*, 448–453. [CrossRef]
39. Mattevi, C.; Kim, H.; Chhowalla, M. A review of chemical vapour deposition of graphene on copper. *J. Mater. Chem.* **2011**, *21*, 3324–3334. [CrossRef]
40. Huang, L.; Chang, Q.; Guo, G.; Liu, Y.; Xie, Y.; Wang, T.; Ling, B.; Yang, H. Synthesis of high-quality graphene films on nickel foils by rapid thermal chemical vapor deposition. *Carbon* **2012**, *50*, 551–556. [CrossRef]
41. Kang, J.; Shin, D.; Bae, S.; Hong, B.H. Graphene transfer: Key for applications. *Nanoscale* **2012**, *4*, 5527–5537. [CrossRef] [PubMed]
42. Hong, S.K.; Song, S.M.; Sul, O.; Cho, B.J. Carboxylic group as the origin of electrical performance degradation during the transfer process of CVD growth graphene. *J. Electrochem. Soc.* **2012**, *159*, K107. [CrossRef]
43. Ambrosi, A.; Pumera, M. The CVD graphene transfer procedure introduces metallic impurities which alter the graphene electrochemical properties. *Nanoscale* **2014**, *6*, 472–476. [CrossRef] [PubMed]

44. Boas, C.; Focassio, B.; Marinho, E.; Larrude, D.; Salvadori, M.; Leão, C.R.; Dos Santos, D.J. Characterization of nitrogen doped graphene bilayers synthesized by fast, low temperature microwave plasma-enhanced chemical vapour deposition. *Sci. Rep.* **2019**, *9*, 13715. [CrossRef]
45. Kim, J.H.; Castro, E.J.D.; Hwang, Y.G.; Lee, C.H. Synthesis of Few-Layer Graphene Using DC PE-CVD. *AIP Conf. Proc.* **2011**, *1399*, 801–802.
46. Childres, I.; Jauregui, L.A.; Park, W.; Cao, H.; Chen, Y.P. Raman spectroscopy of graphene and related materials. *New Dev. Photon Mater. Res.* **2013**, *1*, 1–20.
47. Zafar, Z.; Ni, Z.H.; Wu, X.; Shi, Z.X.; Nan, H.Y.; Bai, J.; Sun, L.T. Evolution of Raman spectra in nitrogen doped graphene. *Carbon* **2013**, *61*, 57–62. [CrossRef]
48. Zheng, S.; Zhong, G.; Wu, X.; D'Arsiè, L.; Robertson, J. Metal-catalyst-free growth of graphene on insulating substrates by ammonia-assisted microwave plasma-enhanced chemical vapor deposition. *RSC Adv.* **2017**, *7*, 33185–33193. [CrossRef]
49. Wang, C.; Yuen, M.F.; Ng, T.W.; Jha, S.K.; Lu, Z.; Kwok, S.Y.; Wong, T.L.; Yang, X.; Lee, C.S.; Lee, S.T. Plasma-assisted growth and nitrogen doping of graphene films. *Appl. Phys. Lett.* **2012**, *100*, 253107. [CrossRef]
50. Merel, P.; Tabbal, M.; Chaker, M.; Moisa, S.; Margot, J. Direct evaluation of the sp3 content in diamond-like-carbon films by XPS. *Appl. Surf. Sci.* **1998**, *136*, 105–110. [CrossRef]
51. Marinoiu, A.; Raceanu, M.; Andrulevicius, M.; Tamuleviciene, A.; Tamulevicius, T.; Nica, S.; Bala, D.; Varlam, M. Low-cost preparation method of well dispersed gold nanoparticles on reduced graphene oxide and electrocatalytic stability in PEM fuel cell. *Arab. J. Chem.* **2020**, *13*, 3585–3600. [CrossRef]
52. JankauskaitĿ, V.; VitkauskienĿ, A.; Lazauskas, A.; Baltrusaitis, J.; ProsyĿevas, I.; AndruleviĿius, M. Bactericidal effect of graphene oxide/Cu/Ag nanoderivatives against Escherichia coli, Pseudomonas aeruginosa, Klebsiella pneumoniae, Staphylococcus aureus and Methicillin-resistant Staphylococcus aureus. *Int. J. Pharm.* **2016**, *511*, 90–97. [CrossRef] [PubMed]
53. He, H.; Yang, Q.; Xiao, S.; Han, X.; Li, Q.; Lv, K.; Hong, J.; Tang, D.; Kejian, D. Investigation of Edge-selectively Nitrogen-doped Metal Free Graphene For Oxygen Reduction Reaction. *J. Adv. Nanotechnol.* **2020**, *1*, 5–13.
54. Tian, K.; Wang, J.; Cao, L.; Yang, W.; Guo, W.; Liu, S.; Li, W.; Wang, F.; Li, X.; Xu, Z. Single-site pyrrolic-nitrogen-doped sp2-hybridized carbon materials and their pseudocapacitance. *Nat. Commun.* **2020**, *11*, 3884. [CrossRef]
55. Liu, F.; Zhang, Z.; Rong, X.; Yu, Y.; Wang, T.; Sheng, B.; Wei, J.; Zhou, S.; Yang, X.; Xu, F. Graphene-Assisted Epitaxy of Nitrogen Lattice Polarity GaN Films on Non-Polar Sapphire Substrates for Green Light Emitting Diodes. *Adv. Funct. Mater.* **2020**, *30*, 2001283. [CrossRef]
56. Wu, Z.; Wang, Y.; Li, S.; Wang, X.; Xu, Z.; Zhou, F. Mechanical and tribological properties of BCN coatings sliding against different wood balls. *Sci. Eng. Compos. Mater.* **2019**, *26*, 402–411. [CrossRef]
57. Zhou, J.; Ye, F.; Cui, X.; Cheng, L.; Li, J.; Liu, Y.; Zhang, L. Mechanical and dielectric properties of two types of Si3N4 fibers annealed at elevated temperatures. *Materials* **2018**, *11*, 1498. [CrossRef]
58. Tao, F.; Wang, Z.H.; Qiao, M.H.; Liu, Q.; Sim, W.S.; Xu, G.Q. Covalent attachment of acetonitrile on Si (100) through Si–C and Si–N linkages. *J. Chem. Phys.* **2001**, *115*, 8563–8569. [CrossRef]
59. Luo, Z.; Lim, S.; Tian, Z.; Shang, J.; Lai, L.; MacDonald, B.; Fu, C.; Shen, Z.; Yu, T.; Lin, J. Pyridinic N doped graphene: Synthesis, electronic structure, and electrocatalytic property. *J. Mater. Chem.* **2011**, *21*, 8038–8044. [CrossRef]
60. Legesse, M.; El Mellouhi, F.; Bentria, E.T.; Madjet, M.E.; Fisher, T.S.; Kais, S.; Alharbi, F.H. Reduced work function of graphene by metal adatoms. *Appl. Surf. Sci.* **2017**, *394*, 98–107. [CrossRef]
61. Sheng, Z.-H.; Shao, L.; Chen, J.-J.; Bao, W.-J.; Wang, F.-B.; Xia, X.-H. Catalyst-free synthesis of nitrogen-doped graphene via thermal annealing graphite oxide with melamine and its excellent electrocatalysis. *ACS Nano* **2011**, *5*, 4350–4358. [CrossRef] [PubMed]
62. Wei, D.; Peng, L.; Li, M.; Mao, H.; Niu, T.; Han, C.; Chen, W.; Wee, A.T.S. Low temperature critical growth of high quality nitrogen doped graphene on dielectrics by plasma-enhanced chemical vapor deposition. *ACS Nano* **2015**, *9*, 164–171. [CrossRef] [PubMed]